Electrochemical Impedance Spectroscopy

Byoung-Yong Chang[1] and Su-Moon Park[2]

[1]Department of Chemistry, Pohang University of Science and Technology, Pohang 790-784, Korea; email: taiji@postech.edu

[2]School of Energy Engineering, Ulsan National Institute of Science and Technology, Ulsan 689-805, Korea; email: smpark@unist.ac.kr

Annu. Rev. Anal. Chem. 2010. 3:207–29

First published online as a Review in Advance on February 25, 2010

The *Annual Review of Analytical Chemistry* is online at anchem.annualreviews.org

This article's doi: 10.1146/annurev.anchem.012809.102211

1936-1327/10/0719-0207$20.00

Key Words

electrochemical measurements, equivalent circuits, electrified interfaces, electrode kinetics, biosensors

Abstract

This review describes recent advances in electrochemical impedance spectroscopy (EIS) with an emphasis on its novel applications to various electrochemistry-related problems. Section 1 discusses the development of new EIS techniques to reduce measurement time. For this purpose, various forms of multisine EIS techniques were first developed via a noise signal synthesized by mixing ac waves of various frequencies, followed by fast Fourier transform of the signal and the resulting current. Subsequently, an entirely new concept was introduced in which true white noise was used as an excitation source, followed by Fourier transform of both excitation and response signals. Section 2 describes novel applications of the newly developed techniques to time-resolved impedance measurements as well as to impedance imaging. Section 3 is devoted to recent applications of EIS techniques, specifically traditional measurements in various fields with a special emphasis on biosensor detections.

1. INTRODUCTION

Electrochemical impedance spectroscopy (EIS) has been known to the electrochemistry community for more than a century; Macdonald (1) recently published an excellent account of its history. Whereas Macdonald wrote that electrical equivalent circuits (EECs) are merely analogs, rather than models, we describe an electrochemical reaction that takes place at the electrode/electrolyte interface, using an EEC as a model. We then examine whether an EEC can indeed be used as a model for the reaction at the electrified interface.

The current flowing at an electrified interface due to an electrochemical reaction,

$$O + ne^- \rightarrow R, \tag{1}$$

always contains nonfaradaic components, no matter how well the measurement is made. In this equation, n is the number of electrons transferred, O is the oxidant, and R is its reduced product (reductant). The electron is transferred across the electrified interface, as illustrated in **Figure 1*a***. The charge transfer leads to both faradaic and nonfaradaic components. The faradaic component arises from the electron transfer via a reaction (1) across the interface by overcoming an appropriate activation barrier, namely the polarization resistance (R_p), along with the uncompensated

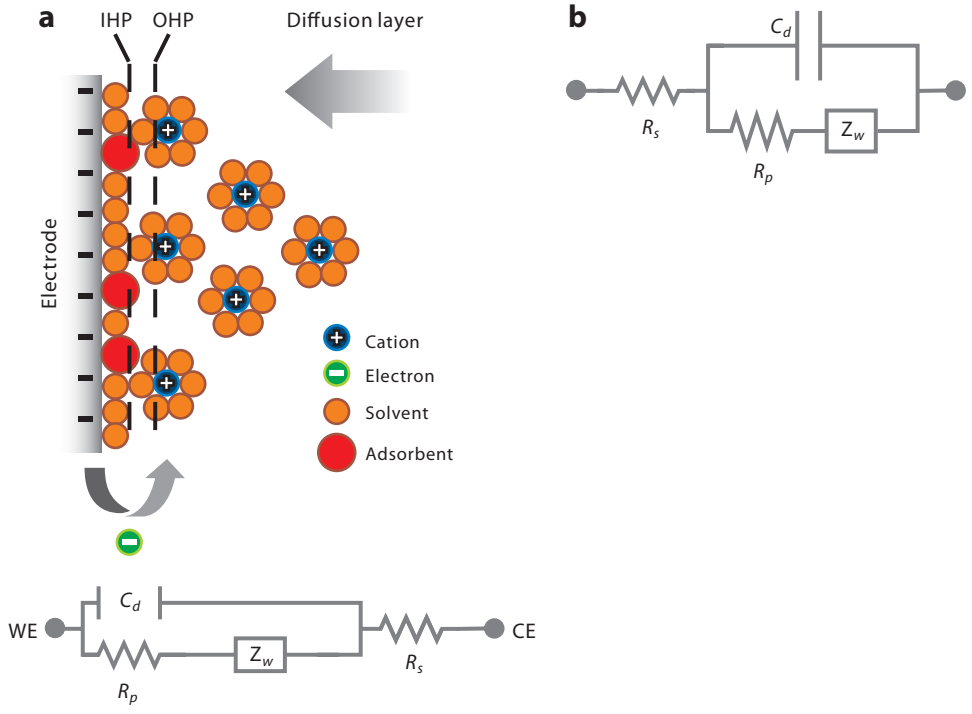

Figure 1

(*a*) At top is an electrified interface in which the electrode is negatively charged; countercations are aligned along the electrified surface. At bottom are the electrical circuit elements corresponding to each interface component. (*b*) An idealized Randles electrical equivalent circuit for the interface, shown with no specifically adsorbed anions. The high-frequency components are shown on the left, and the low-frequency components are shown on the right. Abbreviations: C_d, double-layer capacitor; CE, counterelectrode; IHP, inner Helmholtz plane; OHP, outer Helmholtz plane; R_p, polarization resistance; R_s, solution resistance; WE, working electrode; Z_W, Warburg impedance.

solution resistance (R_s). The nonfaradaic current results from charging the double-layer capacitor (C_d). When the charge transfer takes place at the interface, the mass transports of the reactant and product take on roles in determining the rate of electron transfer, which depends on the consumption of the oxidants and the production of the reductant near the electrode surface. The mass transport of the reactants and the products provides another class of impedance (Z_W), which can be exploited by electroanalytical chemists because it shows up in the form of a peak current in a voltammogram or a current plateau in a polarogram. The EEC in **Figure 1*a*** shows that each circuit component corresponds to each interfacial component. The EEC first proposed by Randles (2), shown in **Figure 1*b***, displays both the high-frequency components (e.g., R_s) and the low-frequency components (e.g., Z_W). The left-to-right arrangement of the EECs is important because the impedance data are normally displayed in this manner (**Figure 2**). Also, note that the activation barrier at any potential is represented by the polarization resistance, R_p, but that the barrier becomes the charge-transfer resistance, R_{ct}, at the standard (or formal) electrode potential.

In efforts to eliminate or minimize the effects of capacitive currents during transient electrochemical experiments, electrochemists have been developing techniques such as normal and differential pulse voltammetry as well as other related methods (3). These techniques are necessary because transient signals obtained from linear sweep or cyclic voltammetry, chronoamperometry, and chronopotentiometry experiments are affected by double-layer charging currents to different extents, depending on the experimental conditions. As shown in **Figure 1**, the environment in which the charge-transfer reaction takes place dictates all the related parameters to be described based solely on the full impedance data obtained during the reaction, given that the traditional electrochemical measurements described above provide only limited information about the system. For complete information about the interface, one must run either several separate traditional transient experiments or an EIS experiment.

The frequency-dependent impedance, $Z(\omega)$, at the interface that has the circuit elements shown in **Figure 1*b*** has a rather complex expression,

$$Z(\omega) = R_s + \frac{R_p + \sigma\omega^{-1/2}}{\sigma\omega^{1/2}(C_d+1)^2 + \omega^2 C_d^2 (R_p + \sigma\omega^{-1/2})^2} + j\frac{[\omega C_d (R_p + \sigma\omega^{-1/2})^2 + \sigma\omega^{-1/2}(C_d\sigma\omega^{1/2}+1)]}{(C_d\sigma\omega^{1/2}+1)^2 + \omega^2 C_d^2 (R_p + \sigma\omega^{-1/2})^2}. \quad (2)$$

Here $\omega = 2\pi f$, where f is frequency, j is $(-1)^{1/2}$, and

$$\sigma = \frac{RT}{\sqrt{2}n^2F^2A}\left(\frac{1}{D_O^{1/2}C_O(x,t)} + \frac{1}{D_R^{1/2}C_R(x,t)}\right), \quad (3)$$

where A is the electrode area, Cs are concentrations of subscripted species at a distance x from the electrode surface, and t is time. The other symbols either are defined above or have their usual meanings. Equation 2 can be simplified to

$$Z(\omega) = R_s + \frac{R_p}{1+\omega^2 R_p^2 C_d^2} - j\frac{\omega R_p^2 C_d}{1+\omega^2 R_p^2 C_d^2} = Z'(\omega) - jZ''(\omega), \quad (4)$$

at high frequencies ($\omega \to \infty$). At low frequencies ($\omega \to 0$), it becomes

$$Z(\omega) = R_s + R_p + \sigma\omega^{-1/2} - j(\sigma\omega^{-1/2} + 2\sigma^2 C_d). \quad (5)$$

The Warburg impedance is related to σ by the equation

$$Z_W = \left(\frac{2}{\omega}\right)^{1/2}\sigma. \quad (6)$$

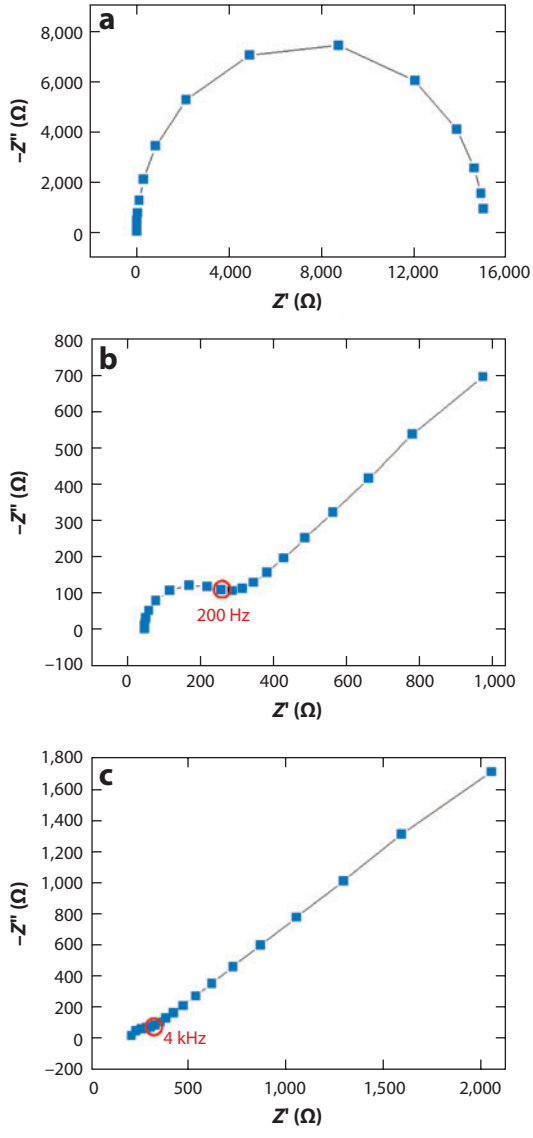

Figure 2

Nyquist plots obtained from Equation 7 with different kinetic parameters. The calculations were performed between 50 kHz and 1 Hz. The $k^0/\sqrt{D}$ values (relative rates of electron transfer to that of mass transfer) used for the calculation were (*a*) 1.0×10^{-3} $s^{1/2}$, (*b*) 1.0 $s^{1/2}$, and (*c*) 1.0×10^{3} $s^{1/2}$. The high-frequency component, R_s, is shown on the left, and the low-frequency component, Z_W, is shown on the right. The intermediate-frequency component (*circles*) arising from R_p and C_d is located in between. Data taken from Reference 45.

Thus, Equation 4 shows that a semicircle with a radius of $R_p/2$, with a high-frequency intercept of R_s and a low-frequency intercept of $(R_s + R_p)$ on the $Z'(\omega)$ axis, is obtained when $-Z''(\omega)$ is plotted against $Z'(\omega)$ (**Figure 2**) (4). In the low-frequency region, however, a straight line with a slope of one and an intercept of $(R_s + R_p - 2\sigma^2 C_d)$ is obtained (**Figure 2*b*,*c***). Thus, one can obtain all the necessary circuit parameters from these plots. More detailed descriptions and derivations

of equations can be found in recent textbooks and monographs (3, 5). Impedance responses under various experimental conditions have been reviewed by Macdonald (1).

Many reviews of EIS have been published in recent years (1, 6–15); however, most of them address applications of EIS as a detection tool for biosensors, biological cell analysis, or clinical analysis (6–14). In this review, we focus on recent advances in EIS techniques and their applications to various fields of studies. Because of space constraints, we cannot cover the topic exhaustively; we apologize for any inadvertent omissions.

2. RECENT ADVANCES IN ELECTROCHEMICAL IMPEDANCE SPECTROSCOPY MEASUREMENT TECHNIQUES AND THEIR APPLICATIONS

2.1. New Forms of Electrochemical Impedance Spectroscopy Measurements

As stated by Macdonald (1), in the early twentieth century EIS experiments were conducted primarily to measure the capacitance of an ideally polarizable electrode such as mercury. Measurements of full impedance spectra were not made until approximately the 1970s, when the use of reliable potentiostats had become widespread. Of the various methods of impedance measurements, the frequency response analyzer (FRA) has become a de facto standard. FRA is a single-sine method in which a small ac wave of 5 to 15 mV of a given frequency is overlaid on a desired dc bias potential and applied to the working electrode; an ac current measurement is then made. This process is repeated by scanning the frequency and computing the impedances from the ac voltage and current data at desired frequencies, typically five to ten measurements for a decade change in frequency. However, this method is viable only for a stable and reversible system in equilibrium, as the system's linearity, stability, and causality must be ensured. For this reason, early investigators questioned the validity of impedance measurements (15–16) and hoped to make instantaneous impedance measurements for nonstationary systems. Stoynov & Savova-Stoynov (17–20) published mathematical expressions to extract instantaneous impedance values for nonstationary systems. Problems with this approach arise primarily from the relatively long data-acquisition time required for the single-sine FRA method.

In efforts to reduce the measurement time, investigators have proposed methods in which no frequency scanning is employed. Smith (21) and others (22–24) used the fast Fourier transform (FFT) method after obtaining the current signal upon application of a noise signal, which was achieved by mixing the ac voltages of various frequencies, to an electrochemical cell. The impedances were then computed from the deconvoluted ac voltages and currents; we term this technique the first-generation Fourier transform EIS (1-FTEIS) method. Recently, Popkirov & Schindler (25) simplified this technique and implemented it into an EIS spectrometer through use of a noise signal obtained by mixing the ac waves of 42 appropriate frequencies. When the low-frequency limit of the ac voltage is reasonably high at 10 Hz, for example, it takes approximately 0.1 s to obtain a full impedance spectrum, although the number of data points is limited.

A few other groups have adopted or further developed the simplified method (1′-FTEIS). Baranski et al. (26) used the mixed multisine ac voltage signal with frequencies ranging from 5 kHz to 5 MHz to impedance measurements at a microelectrode and reported a data-acquisition time of less than 5 ms. Rosvall & Sharp (27) developed a slightly more sophisticated form by combining the multisine signal with staircase voltammetry, in which a wavelet consisting of mixed sinusoidal waves of 20 frequencies between 150 Hz and 200 kHz was overlaid on the latter part of the step during the staircase voltammetry experiment. A number of other studies, in which the 1′-FTEIS method was combined with cyclic voltammetry (28–41), soon followed.

Darowicki et al. (28) validated the 1′-FTEIS method using a wavelet of seven ac frequencies ranging from 60 to 997 Hz to record impedances of a nonstationary electrical system. This system consisted of a capacitor and a diode connected in parallel and was polarized at a constant rate in the conduction direction of the diode. After verifying that the method provided true impedance signals, the authors coupled the method with cyclic voltammetry by overlaying the wavelet on a slow ramp signal. They later termed this technique dynamic electrochemical impedance spectroscopy (DEIS) (28–30). Darowicki et al. later used this method to study various electrochemical phenomena, including corrosion of metals such as aluminum and stainless steel (31–33) and the appearance of anodic excursion peaks from a lead-acid battery (34). They also developed a method with which to monitor the local impedances of a 0.1-mm-thick polymer membrane [polyvinylchloride plasticized with bis(2-ethylhexyl) sebacate and doped with tetradodecylammonium tetrakis(4-chlorophenyl) borate] using a steel electrode with a tip diameter of 0.1 mm.

Several other groups have contributed to the development of FTEIS. For example, Roy and colleagues (36) studied the underpotential deposition (UPD) of Bi^{3+} in the presence of ClO_4^- by employing 1-FTEIS (which they termed FFT-EIS). The authors claimed to have simultaneously probed both the steady-state and transient behaviors of the interface. They also reported time-resolved impedance spectra for a gold electrode, describing considerations for running such experiments as well as the hardware requirements for data acquisition (37). Later, the authors conducted a more detailed analysis of the kinetic parameters for faradaic and nonfaradaic reactions on thin films on gold (38). They used a scan rate of 5 mV s^{-1} and a multisine signal of 65 sinusoidal waves with a frequency range of 100 Hz to 10 kHz on the dc ramp signal. Ragoisha & Bondarenko (39) conducted similar experiments, which they termed potentiodynamic electrochemical impedance spectroscopy (PDEIS), on a quasi-reversible redox system, $Fe(CN)_6^{3-/4-}$. They applied the technique to, for instance, identification of the capacitances of TiO_2 films for Mott-Schottky plots (40) and studies of the lead UPD on polycrystalline gold as well as on the selenium atomic underlayer (41).

The Park group (42–51) developed an approach that was entirely different from those that had been used thus far. In their experiments, a small step signal, instead of mixed sinusoidal waves, was applied to a working electrode at a given dc bias voltage, and the resulting chronoamperometric current was recorded. The step signal is an integrated form of the Dirac δ function, which is obtained by summing the ac voltages of all frequencies. In this process, derivative signals obtained from both the voltage step and the recorded current signals were deconvoluted into ac voltages, and the currents were deconvoluted into the frequency domain by the FFT method. The impedance at a desired frequency was first obtained by dividing an ac voltage at that frequency by the current at the frequency. A full impedance spectrum was then constructed by repeating the calculation through the frequency range. We term this technique second-generation Fourier transform EIS (2-FTEIS) because true white noise (δ) containing ac waves of all frequencies is used as an excitation signal, just as in Fourier transform infrared spectroscopy or nuclear magnetic resonance experiments.

There were several assumptions and requirements for this series of operations. The most important and stringent requirements for hardware were (*a*) that the potentiostat be fast rising to transmit the well-defined step signal to the cell and (*b*) that the data-acquisition system not only be fast enough to ensure recording high-frequency data but also have a high bit resolution so that low-frequency data could be recorded with high precision. Details of the other assumptions and requirements for the system are given in Reference 42. The Park group took measurements at a given dc bias potential by applying a small voltage step signal of 5 to 20 mV and recording the resultant current for the step period of a few milliseconds to as long as a few seconds. The highest frequency was $1/(2\cdot\Delta t)$, and the lowest was $1/(n\cdot\Delta t)$, where Δt is the signal-sampling interval, n is the total number of samples, and $n\cdot\Delta t$ is the step period t_p (52). Although the authors initially

conducted the experiments at specified dc bias potentials, they later coupled the experiments with staircase cyclic voltammetry to obtain both EIS data as a function of potential and staircase cyclic voltammograms (SCVs). Thus, a series of ascending and/or descending voltage steps were applied to the cell, and each step produced a full impedance spectrum (43) in a frequency region ranging from $1/(2\cdot\Delta t)$ to $1/t_p$. For example, for an experiment with a step period of 150 ms with a 1-MHz sampling frequency, an impedance spectrum would be obtained in a frequency range of 50 kHz to 6.7 Hz in 0.15 s. The authors validated the impedance data by conducting the Kramers-Krönig transform operation (53). Thus, these SCV-FTEIS experiments allowed truly time-resolved impedance spectra to be recorded as a function of time at every stepped potential while SCVs were recorded. Note that an SCV recorded by connecting currents sampled at a sampling time t_p is equivalent to a cyclic voltammogram (CV) recorded at a scan rate of $\Delta E/4t_p$, where ΔE is the step height (54); the current sampling time does not need to be the same as t_p. Thus, scan rates as fast as a few hundred millivolts per second can be used while the impedance spectra are obtained in real time. The scan rate can be much faster, provided that only high-frequency data are acquired.

Another important conclusion reached from the above-described studies was that the EEC is not merely an analog capable of simply fitting the impedance data, as had been described by Macdonald (1); rather, it can serve as a true model for an electrochemical reaction. To demonstrate this point, Chang & Park (45) derived the following expression for the current obtained upon applying a potential step, ΔE, across the EEC shown in **Figure 1*b***,

$$i(t) = \frac{-\Delta E}{R_p + R_s} \cdot \exp\left[\left(\frac{\sqrt{2}\sigma}{R_p + R_s}\right)^2 \cdot t\right] \cdot \operatorname{erfc}\left[\frac{\sqrt{2}\sigma}{R_p + R_s} \cdot \sqrt{t}\right] + \frac{-\Delta E \cdot R_p}{R_s(R_p + R_s)} e^{-\frac{(R_p + R_s)}{R_p R_s C_d} \cdot t}, \quad (7)$$

by using the impedance expression shown in Equation 2. In this equation, exp and erfc refer to exponent and error-function complement, respectively. Surprisingly, the faradaic term of Equation 7, which was obtained for the EEC, has exactly the same form as the current expression that Delahay (55) obtained by solving diffusion equations for a potential step:

$$I_f = nFA(k_f \cdot C_O^* - k_b \cdot C_R^*) \cdot \exp(H^2 t) \cdot \operatorname{erfc}(H\sqrt{t}). \quad (8)$$

Here H is defined as

$$H = \frac{k_f}{\sqrt{D_O}} + \frac{k_b}{\sqrt{D_R}}, \quad (9)$$

where k_f and k_b are the forward- and reverse-rate constants, respectively, for the electron-transfer reaction (1) and D is the diffusion coefficient of the subscripted species. Thus, the current expression obtained for the EEC and the solution process for the same experiment have the same form and produce identical currents when computed via two equations (45). Also, note that Equation 7 contains the nonfaradaic expression as its second term; the EEC indeed represents a real model for the electron-transfer reaction.

After deriving the above expression, Chang & Park (45) computed impedances using Equation 7 for different H values and obtained the results shown in **Figure 2**. The Nyquist plot in **Figure 2*c*** shows that the Warburg line dominates the impedance plot for a reversible electrochemical system such as $Ru(NH_3)_6^{3+/2+}$ and ferrocene/ferrocenium pairs. In such systems, the mass transport is rate limiting due to the very fast charge-transfer rate; thus, use of frequencies higher than 1 kHz is justified for recording a full impedance spectrum, including a Warburg line. This conclusion suggests that the step period can be as short as 1 ms (1 kHz) to record a full spectrum. However, only a semicircle is obtained, and no Warburg impedance is displayed, when the charge-transfer

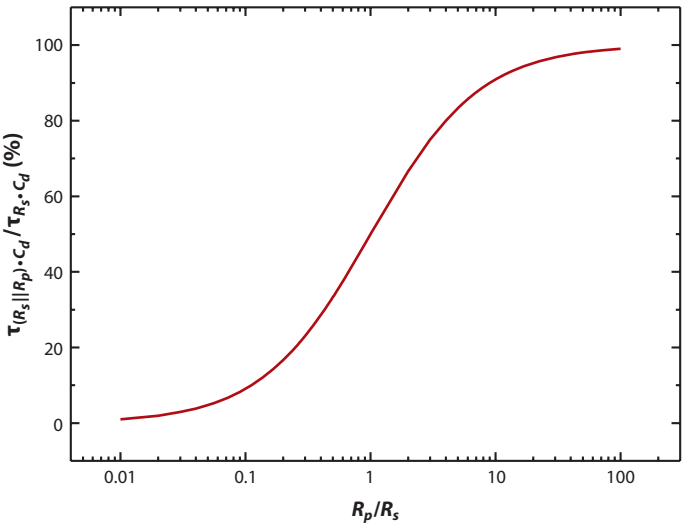

Figure 3

Ratio of the time constants plotted for the ratio of R values obtained from the parallel connection of R_p and R_s ($\tau_{(Rs\|Rp)\cdot Cd}$) to the ratio calculated with R_s alone ($\tau_{Rs\cdot Cd}$). Data taken from Reference 45. Abbreviations: C_d, double-layer capacitor; R_p, polarization resistance; R_s, solution resistance.

rate is much smaller in comparison to the $D^{1/2}$ value. In such cases, one may need to increase both the overpotential and the ΔE value in the SCV-FTEIS experiment.

Examination of the nonfaradaic term of Equation 7 also indicates that the system time constant (τ) acts as if the two circuit components, R_p and R_s, were connected in parallel rather than in series, as electrochemists have so far assumed. As a result, the capacitive currents can be significantly different depending on how large or small the R_p value is in comparison to R_s. Prior to the start of the electron-transfer reaction, the time constant is determined only by R_s, but both R_s and R_p values begin to play a role when the potential reaches a value at which R_p competes with R_s. At a very large overpotential, the contribution from R_p dominates the time constant that would have been obtained from a serial connection of R_s and C_d, namely an R_sC_d time constant. **Figure 3** shows how the system's time constants behave, depending on the situation. Our present understanding of the time constant of an electrochemical system is incorrect, although the difference may not be significant for some cases.

Chang & Park (47) later demonstrated that it is possible to completely describe the electrified interface through use of the impedance data acquired from a single pass of the SCV-FTEIS experiment. To do so, one must obtain all the necessary reaction parameters such as (*a*) kinetic parameters, including the exchange-rate constant ($k°$) and the transfer coefficient (α); (*b*) thermodynamic parameters, including $E_{1/2}$ and n; and (*c*) the mass-transport parameter (D). The kinetic parameters are obtained simply by plotting a series of R_p values as a function of the scanned potential according to the Butler-Volmer or Tafel equation. To obtain the thermodynamic and mass-transport parameters, the expression for σ can be expanded to

$$\sigma = \frac{RT}{\sqrt{2}n^2F^2AD_O^{1/2}C_O^*}\left\{\frac{1}{\xi}\exp\left[-\frac{nF}{RT}(E-E_{1/2})\right]+2+\xi\exp\left[\frac{nF}{RT}(E-E_{1/2})\right]\right\}, \qquad (10)$$

where ξ is $(D_O/D_R)^{1/2}$. Examination of the Warburg admittance obtained from Equation 6 reveals that the admittance reaches a maximum at $E_{1/2}$, providing the $E_{1/2}$ of the reaction. The n and D

values are also obtained from the ac admittance voltammogram. This simple way of describing an electrochemical system has been applied to studies of various reaction systems such as earlier phases of electrochemical polymerization of aniline (48), resolution of multielectron-transfer steps during sulfur reduction (49), UPD of lead on gold (50), and diffusional electrochemistry of cytochrome *c* on a self-assembled monolayer (SAM)-covered electrode (51).

Several groups of investigators employed Laplace transform, instead of Fourier transform, beginning as early as the 1970s (56–60). The general principle of this technique is similar to that for the Fourier transform method. An appropriate perturbation signal—either the voltage or the current step—is applied to the working electrode, and the impedance is obtained from the response of the cell according to

$$Z_L = \frac{V(s)}{I(s)} = \frac{\int_0^\infty v(t)e^{-st}dt}{\int_0^\infty i(t)e^{-st}dt}, \quad (11)$$

where Z_L is the Laplace impedance function; $v(t)$ and $i(t)$ are the voltage and current functions in the time domain, respectively; and $s = \alpha + j\omega$, where α is a convergence parameter of the real number. Note that either $v(t)$ or $i(t)$ can be a perturbation signal and that the other can be a response, depending on the type of cell (58, 60). Although the corresponding Fourier transform does not converge for a voltage step begun at $t = 0$, the Laplace integral shown in Equation 11 does converge when α is large enough. Details of experiments and evaluations of the impedances in frequency domain have been described in the literature for studies of both battery electrodes (58–60) and the corrosion of metals (57).

2.2. Applications of First- and Second-Generation Fourier Transform Electrochemical Impedance Spectroscopy Techniques

Numerous interesting applications have evolved from the EIS experiments on various electrochemical problems that could not have been solved without the new methods described above. Electrochemists have long desired to record impedance spectra fast enough to resolve the changes that take place at the interface. In this section, we describe how FTEIS techniques are applied to studies on biosensors, complex reaction mechanisms, UPDs, corrosion reactions, surface changes, and semiconductor materials.

Park et al. (61, 62) demonstrated that their FTEIS technique can serve as a more sensitive time-resolved detection tool than can its voltammetric counterpart for biosensors. Impedances were monitored during a reaction whose product changed the charge-transfer rate for an electrochemical redox probe. The neurotransmitter serotonin was effectively captured by the host cavities of a (*R*)-lipo-diaza-18-crown-6 SAM on gold electrodes through the formation of a host-guest complex; the SAM provided molecular cavities of the correct size for the serotonin molecule by housing it in the compound 18-crown-6. The captured serotonin molecules facilitated the charge-transfer rate for the $Fe(CN)_6^{3-/4-}$ redox probe, the degree of which depends on the serotonin concentration in solution. **Figure 4** shows the sensing scheme, the potential program, and a series of the simultaneously monitored signals for the reaction via CV and EIS measurements during the reaction. The two experiments were conducted in series via the potential programmed, as shown in **Figure 4*b***. A 10-mV-potential step was used for the first 2.5 s, followed by a cyclic ramp signal for the next 2.5 s. An impedance spectrum was recorded for the first 2.5 s (down to 0.40 Hz), and a CV was obtained at a scan rate of 40 mV s^{-1} while the reaction proceeded. The CVs show that only their reversibility improved and that there were almost no changes in their peak currents (**Figure 4*d***), whereas the impedance spectra underwent significant changes over time (**Figure 4*c***). These results clearly indicate that the process of recording EIS spectra is a

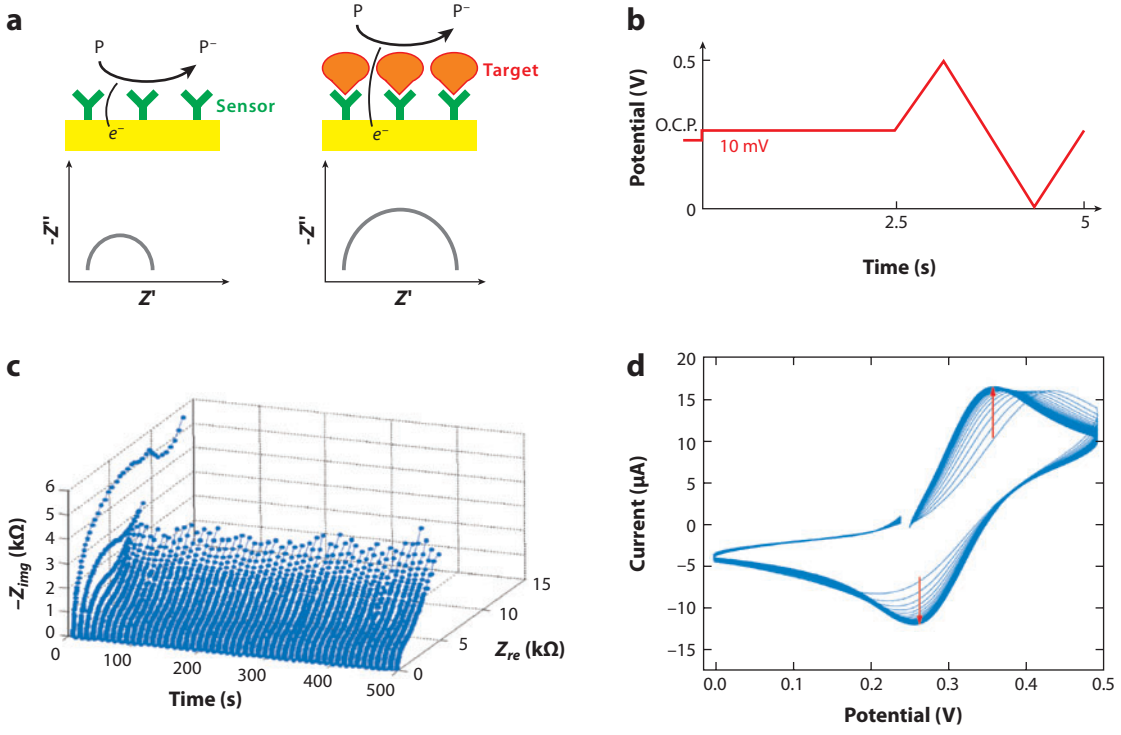

Figure 4

(*a*) General scheme for label-free detection via electrochemical impedance spectroscopy (EIS). The charge-transfer impedance for the probe ions (P) is increased due to the target analyte bound to a proper sensing platform. (*b*) Potential program to sequentially acquire both Fourier transform EIS (FTEIS) and cyclic voltammogram (CV) data. First, a potential step of 10 mV is applied on the dc bias of 0.245 V for 2.5 s. Second, a ramp signal, with upper and lower vertex voltages of 0 to 0.50 V and a scan rate of 400 mV s^{-1}, is applied. (*c*) Series of FTEIS spectra. (*d*) CVs obtained as a function of time upon injection of 400 μl of 1 mM serotonin to 4 ml of the probe solution. Data taken from Reference 61.

much more sensitive detection tool than is the process of recording CVs for monitoring analyte concentration. This is also true for the reaction of glycated hemoglobin (HbA_{1c}) with boronic acid on the thiophene-3–boronic acid SAM-covered gold electrode (62).

Scientists are eager to apply their techniques to solving problems to demonstrate their utility, and the investigators involved in developing 1-FTEIS are no exception. Darowicki & Slepski (30) examined the well-known electrochemical reaction involving reduction of Cd^{2+} at a hanging mercury electrode, and they characterized the reaction in terms of R_p and C_d, along with Warburg coefficients, as a function of reduction potential. Both the R_p and the Warburg coefficient went through a minimum at $E_{1/2}$, whereas the C_d value increased in the same manner as a polarogram would. Similar observations were reported by other investigators, who provided additional interpretable parameters by converting the circuit parameters into the electrode-reaction parameters (36, 38, 46, 47). Furthermore, several researchers used this technique to probe more complex reactions, including electrochemical oxidation of aromatic amines to produce conductive polymers (43, 48, 63) such as polyaniline and poly(*o*-theoxyaniline). A series of potential-dependent impedance spectra revealed that different EECs are needed in different potential regimes. This is because the electrical environment of the interface changes during the potential scan as the conductive polymer forms films on the electrode surface; this process may impart what is termed

the autocatalysis for oxidation of the monomers. The authors made detailed kinetic analyses while the potential was being scanned (48).

Problems related to the UPD of a few metal ions have also been addressed by a few groups (41, 64–67), who concluded that the reason the FTEIS techniques may serve as a powerful tool is because they allow one to monitor changes in capacitances during the potential scan. The substrates studied included metal-chalcogen atomic multilayers as well as UPDs of Te, Se, Pb, and Cu. The effects of an organic additive on copper deposition have also been addressed (66). A real-time impedance study of a Pb UPD on polycrystalline gold, conducted while the potential was scanned, indicated that the Pb^{2+} adsorption initially followed the Langmuir model and that it was taken up by the Frumkin adsorption when the population of adsorbates became large enough to allow the ions to interact with one another (50).

Another type of reaction that has received attention is metal corrosion (31–33, 67–72). Darowicki et al. (31) used the DEIS technique to study the passive-layer cracking process of aluminum alloys and the dissolution process of stainless-steel specimens (32, 33). The corrosion of stainless-steel samples was studied by Nagarajan et al. (69) and Nagarajan & Rajendran (71) under different solution environments. Roy and colleagues (68) reported on the effects of adsorbing ions such as I^- on Cu, on the chemical-mechanical planarization of copper with surfactants present (67), and on tantalum in oxalic acid solutions (72).

This technique has also been applied to studies of semiconductor electrodes (40, 73–75). Bondarenko & Ragoisha (40) used PDEIS to monitor the potential-dependent capacitances of the space-charge layer of a cathodically treated TiO_2 film. The capacitance data were used to obtain Mott-Schottky plots, which allowed the characteristics of the film, such as doping levels and flat-band potentials, to be determined. Phenomena such as oxide growth on silicon (73), pore etching (74), and pore growth (75) have also been studied through use of these new impedance-measurement techniques.

2.3. Impedance Imaging and Time-Resolved Measurements

Investigators first began recording and mapping local impedances as early as in 1992 (76), and additional reports followed in the same decade (77, 78). Researchers measured local impedances by arranging the tips of two parallel, microsized electrodes located vertically above the specimen electrode and scanning across it after applying small ac waves between the large working electrode and counterelectrode (76). The difference in ac voltage between the microelectrodes and the solution ac current, along with the distance between the tip electrodes and the solution conductivity, led to the acquisition of the local impedance of the working electrode. By moving the two probe electrodes and making impedance measurements at several frequencies, the authors (76) obtained an impedance image of the working electrode. Other groups applied similar approaches to a microtip protruding below a small ring electrode encompassing it (77, 78). These approaches have also been used to map pit growth (78) and the delaminated areas beneath organic coatings (79). Later, Frateur et al. (80) addressed the experimental issues associated with the local impedance by making measurements of the local interfacial impedances at two heights above the electrode surface.

Another approach to impedance imaging involves scanning electrochemical microscopy (SECM) (81–86). In a typical example (shown in **Figure 5*a***), Ervin et al. (81) obtained an impedance image by rastering a glass-sealed conical platinum tip with an approximately 1-μm radius above the polycarbonate membrane surface containing conical shaped pores; they simultaneously measured the total impedance between the tip and a large platinum counterelectrode located on the opposite side of the membrane. The image contrast was obtained due to the decrease

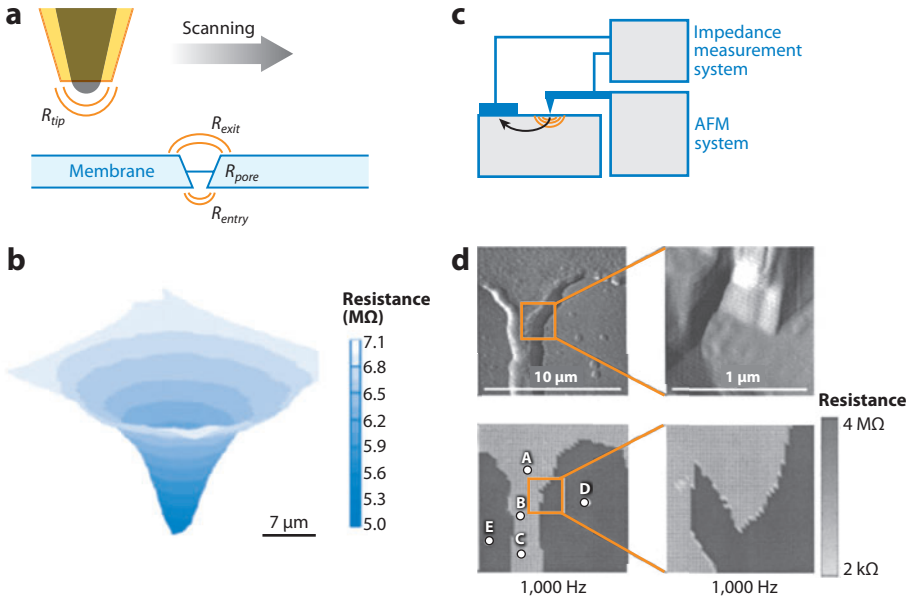

Figure 5

Impedance imaging of two-dimensional surfaces via scanning probes. (*a*) Scheme for impedance imaging of a cone-shaped pore in the polycarbonate membrane by scanning electrochemical microscopy. (*b*) An impedance image for a conical pore. (*c*) Simultaneous atomic force microscopy (AFM) impedance and topography-imaging experiments. (*d*) Shown in the top row are the AFM topographic images of a gold/silicon nitride pattern; shown in the bottom row are corresponding impedance images measured with 1000 Hz ac waves at 0 V dc bias. Panels *a* and *b* are reproduced from Reference 81; panels *c* and *d* are reproduced from Reference 88.

in resistance between the tip and the membrane (**Figure 5*b***). The sensitivity of the measurements was enhanced through use of a low-impedance electrical shunt (i.e., a salt bridge) across the membrane (82). Diakowski & Baranski (83) used SECM measurements to map the conductive and insulating surfaces by analyzing positive and negative ac feedback currents, which depended on experimental conditions. By combining atomic force microscopy (AFM) with alternating current SECM (AC-SECM), Schuhmann and colleagues (84, 86) developed a method that maps the local electrochemical properties at the electrode/electrolyte interface as well as the topography of the substrate. They showed that AC-SECM approach curves toward the conducting substrate can result in either positive or negative feedback responses, depending on the frequency and the topography of the substrate. The AC-SECM technique has recently been reviewed (85).

In 2003, Layson et al. (87) made the first nanoscale impedance measurements on an ionic conductive polymer [poly(ethylene) oxide] surface using a current-sensing AFM (CS-AFM). The measurements were made at several spots on the polymer surface, with a nickel foil on the other side of the film, in a frequency range of 10 kHz to 400 Hz after the topographic image was obtained. Notably, the resistance measured vertically to the film increased by only two orders of magnitude with a decrease in the contact area of the CS-AFM probe by approximately ten orders of magnitude. Similar measurements on ZnO varistors and Nafion® membranes (88) were reported; impedance and topographical images were presented with a spatial resolution approaching approximately 10 nm (as shown in **Figure 5*c*,*d***). Building an image is time consuming, as one must scan both

the frequency and the surface and record the impedance signals. For this reason, Darowicki et al. (89) later combined the DEIS technique, in which 20 ac waves with frequencies ranging from 700 to 44,900 Hz are measured, with the CS-AFM technique in order to map the impedances of a Prussian blue–covered gold surface.

Finally, we describe efforts to develop time-resolved EIS as the speed of recording EIS spectra increases (also see Section 2.1) (33, 37, 43). Schiller et al. (90) demonstrated that enhanced mathematical techniques are necessary for evaluation of EIS spectra that change with time. Quasi-causal spectra were obtained due to the changing states of the polymer electrolyte fuel cell under constant load during the electrolysis reaction. This report, as well as earlier publications describing the stationarity requirements of EIS measurements (17–20), indicates that EIS spectra recorded as a function of time from a system undergoing changes during electrolysis may not represent true impedances unless the rate of measurement is faster than the rate of change.

As mentioned above, electrochemists have attempted to record time-resolved EIS spectra since the early stages of FTEIS development (33, 37, 43, 90). To record time-resolved EIS spectra during a cyclic voltammetric scan in DEIS or PDEIS experiments, one should use a potential scan slower than 10 mV s^{-1} because of hardware constraints (38). In an SCV-FTEIS experiment, however, Yoo et al. (43) demonstrated that the impedances recorded in real time during a voltage scan rate of 240 mV s^{-1} met the Kramers-Krönig transform validity tests. Later studies revealed that scan rates as fast as a few hundred millivolts per seconds could be used while the EIS spectra were being recorded in real time (46–48). In their typical application as a detection tool for biosensors, both CVs and EIS spectra were recorded back to back for the purpose of comparison (61, 62). Whereas the EIS spectra were obtained every 2.5 s in the reports, the measurement time could be decreased significantly, depending on the reversibility of the redox reaction.

3. ELECTROCHEMICAL IMPEDANCE SPECTROSCOPY AS A LABEL-FREE DETECTION TOOL FOR BIOSENSORS

During the past few years, impedance measurements have become increasingly popular as a label-free detection tool for many different types of biosensors (6–10). In experiments employing impedance measurements, the biosensor is prepared on an electrode such that the electron-transfer rate is selectively modulated by the analyte. Although many different chemical reactions may be used to modify the electrode surface, SAMs with appropriate functional groups that selectively capture specific analytes are the most frequently employed technique because they are easy to immobilize and have complete blocking capabilities and stabilities. A typical biosensor may be prepared by dipping a gold electrode in a solution containing (*a*) an organic compound with a thiol group on one side and (*b*) a functional group capable of selectively capturing a target analyte on the other side. The SAM that forms on the gold electrode via covalent binding with the thiol group modulates the electrical and electrochemical environments of the interface; changes in the interfacial environments are detected in the form of changes in capacitances or in charge-transfer rates. These properties are further modulated upon capture of the analyte by the functional group facing the solution. The changes can be detected by voltammetric, amperometric, or impedometric measurements. The selectivity is provided via an appropriate functional group of the molecule forming the SAM, and the analyte is detected by an electrochemical method and does not have to be labeled. In a typical fluorometric method of detection, an efficiently fluorescing group or compound must be labeled onto the analyte before it is analyzed so that the fluorescence intensity of the labeled analyte is related to its concentration.

These types of biosensors detect the changes in electrochemical and/or electrical properties that are caused by the blocking ability of SAMs and SAM-analyte adducts. Ganesh et al. (91)

showed through impedance measurements that the charge transfer occurs to/from an electrode covered by a SAM formed from thiophenol, *o*-aminothiophenol, or *p*-aminothiophenol from/to a $Fe(CN)_6^{3-/4-}$ redox probe through the pinholes and defects of the monolayer, whereas tunneling of electrons is responsible for the $Ru(NH_3)_3^{3+/2+}$ pair. Thus, the extent to which the electrode surface is blocked controls the pinholes as well as the tunneling ability, determining the charge-transfer rate. Depending on what is on the surface, the charge-transfer rate may be enhanced by the SAM instead (61, 92).

Berggren et al. (93) constructed capacitive biosensors for antibodies, antigens, proteins, DNA fragments, and heavy metal ions with detection limits as low as 10^{-15} M by modifying electrode surfaces with SAMs or SAM-analyte adducts, causing dielectric properties of the SAM layers to change. A similar sensor was constructed for the detection of *Escherichia coli* and *Salmonella typhimurium* on digitated gold electrodes, which were functionalized by anchoring biotinylated polyclonal anti–*E. coli* antibodies to a neutravidin-coated surface (94). The electrochemical impedance and capacitance signals in the biosensor were shown to be significantly amplified through gold nanoparticle conjugation for the model fluoroscein-antifluoroscein system (95). Capacitive signals were also shown to be modulated by changes in the thickness or the dielectric constant of the total insulating layer (96). An impedance biosensor for Ara h 1, one of several allergenic proteins found in peanuts, was also constructed on a gold electrode following immobilization of its antibodies (97). The change in differential capacitance was then monitored, although the change in charge-transfer resistance showed greater sensitivity.

Although in several cases changes in interfacial capacitances have been shown to be related to analyte concentrations, changes in the charge-transfer rate generally show greater sensitivity. In this case, an appropriate antibody molecule such as C-reactive protein (CRP) is anchored on a SAM whose surface contains a good host molecule such as (*R*)-lipo-diaza-18-crown-6 (98). The antibody-immobilized electrode is then exposed to the solution containing the analyte (CRP). As the electrode surface is progressively modified by more than one step, the charge transfer across the electrode-electrolyte interface to a redox probe present in the solution becomes increasingly difficult due to the blocking effect of the SAM, antibodies, and antigens. Usually, a redox probe such as $Fe(CN)_6^{3-/4-}$, $Ru(NH_3)_6^{3+/2+}$, or a *p*-benzoquinone/hydroquinone redox pair is used to monitor the modified electrode's ability to transfer electrons. The selection of the redox probe depends on various parameters; thus far, the $Fe(CN)_6^{3-/4-}$ pair has been the most frequently used probe for a number of reasons. Usually, either the charge-transfer rate or the polarization resistance R_p is obtained at equilibrium or formal potential ($E^{0'}$). This allows the charge-transfer resistance R_{ct}, measured at $E^{0'}$, to be compared for different analytes and their concentrations; these comparisons allowed the construction of an immunosensor for small proteins such as CRP and ferritin (98). CRP immunosensors have also been constructed through covalent conjugation of CRP antibodies with 3–mercaptopropionic acid on a three-dimensionally ordered, macroporous, gold film–modified electrode (99). Similarly, a p53 protein sensor was constructed through use of a (*R*)-lipo-diaza-18-crown-6 SAM (100). Sensors for other proteins, including myelin basic protein (101) and prostate-specific antigen (102), have been constructed in a similar manner, except that the polyaniline film rather than the SAMs was used to immobilize respective antibodies. Although in these cases antibodies were used as receptors for the corresponding antigens, a so-called covalent virus layer obtained by the phage-display technique acts as a receptor for a 148.2-kDa antibody (103). O'Grady & Parker (104) controlled protein-protein interactions in the antibody-doped polypyrrole layer by changing the voltage applied to the polymer layer and by monitoring impedances at different potentials. Physically large analytes such as bacteria (105, 106), as well as cell deaths (107), have been counted via similar strategies. In fact, sensors for small analyte molecules such as fluoroquinolone antibiotics (108, 109) and polyamines (110)

have been constructed on the basis of these principles. Note, however, that the R_{ct} values for the $Fe(CN)_6^{3-/4-}$ probe did not increase but rather decreased, as was observed in earlier studies in which the polyamine concentration was increased (111). This peculiar behavior arises from the positive charges of protonated polyamines captured by calyx[4]crown-5, which facilitates the approach of probe ions by electrostatic forces for easier electron transfer. Park et al. (61) obtained similar results for a serotonin sensor that used an (*R*)-lipo-diaza-18-crown-6 SAM in which the serotonin molecule captured inside the cavity had a positive charge.

Note that, in addition to the label-free detections described above, analytes have also been detected after being labeled with an electroactive group such as ferrocene. Mahmoud & Luong (111) recently reported an assay format based on the immobilization of a thiol-terminated ferrocene-pepstatin conjugate on a single-walled carbon nanotube/gold nanoparticle–modified gold electrode. In this format, the alteration of the interfacial properties of the electrode upon interaction between the HIV-1 protease and the Fc-pepstatin conjugate was monitored by EIS measurements.

DNA hybridization, single-nucleotide mismatches, and DNA's interactions with other molecules remain popular subjects following Barton and colleagues' (112) comprehensive review on electrochemical DNA hybridization sensors. DNA analysis generally follows the same protocol as do analyses for the other biosensors described above: DNA's hybridization on the electrode leads to a much more crowded surface than that covered by single-stranded DNA. Also, highly populated negative charges that arise from phosphates linking DNA bases of hybridized double-stranded DNA render the interface hostile to approaching anionic-probe ion pairs, namely $Fe(CN)_6^{3-/4-}$. Such ion pairs modulate the electrode's capability to transfer electrons to the redox probe, and R_{ct} values increase significantly at double-stranded DNA–covered electrodes compared to single-stranded DNA–covered electrodes. This is also true for DNA hybridization at exotic interfaces, such as immiscible liquid-liquid (113) and gold-SiO_2-water (114) interfaces. Interestingly, the DNA hybridized at the liquid-liquid interface significantly enhanced ion-transfer admittances (113).

Through the use of appropriate strategies, a target DNA that has a single mismatch with the probe DNA can be distinguished from its fully complementary target DNA. For example, differences among the charge-transfer abilities of native B-DNA–covered electrodes and metal ion–bound M-DNA–covered electrodes in the absence and presence, respectively, of Zn^{2+} at pH $\geq$ 8.6 allowed unequivocal detection of all eight single-nucleotide mismatches within a 20-mer DNA sequence (115, 116). A small molecular ligand, naphthyridine-azaquinolone, was also found to bind to the G-A region of the mismatch. This binding caused significant changes in the structure of the DNA, which in turn caused changes in the electrochemical properties of the DNA/naphthyridine-azaquinolone films (117). An alternative approach is to secure just enough space for more efficient DNA hybridization via a SAM made of cone-shaped dendron that generates mesospacing (average 3.2 nm) on the surface (118). In this case, the single mismatch at the middle of the target DNA chain was distinguished from that at the end. The dendron-based SAM has an advantage over other thiol-based SAMs in that the distance between each probe DNA is so well defined as to allow effective hybridization with much fewer kinks, less nonspecific adsorption, and less crowdedness of probe DNA molecules; the last problem is to be expected when the probe DNA is immobilized on the thick forest of thin alkyl thiols. Finally, sensors for DNA-binding drugs have been constructed on a gold electrode modified with gold nanoparticles (119), and physically adsorbed double-stranded DNA molecules on polypyrrole nanofibers can act as a spermidine sensor (120).

Label-free aptamer-based sensors employ strategies similar to those of the biosensors described above. In a label-free aptamer-based sensor, the electrode surface is modified by an aptamer showing selective binding to a specified analyte; impedance measurements are made before and

after the electrode is exposed to the solution containing an analyte. Several laboratories have used this procedure to construct thrombin sensors (121–124). The subject has recently been reviewed (125, 126).

4. OTHER APPLICATIONS

The electrochemistry community has long been interested in the use of EIS measurements to solve various complex electrochemical problems. Because this review is intended primarily for analytical chemists, in the section we compile a short list of recent reports on applications of EIS measurements to areas other than biosensors. The primary purpose of EIS applications has been to use impedance data to work out EECs under given experimental conditions, which in turn has allowed the elucidation of the mechanisms of related reactions.

EIS has been applied to the dissolution of metals (127), corrosion inhibition (128–131), evaluation of corrosion rates (132), and corrosion protection by polymer coatings (133). Hardware requirements (133) and acquisition of corrosion rates from polarization measurements (132) have recently been reviewed in detail. Another area of interest is the study of complex electrochemical reactions such as electrochemical synthesis of conducting polymers (134–136) and their product characterization (137) and degradation (138). The EECs obtained for these reactions from the impedance data acquired by single-sine or 1-FTEIS methods represent time-averaged results over relatively long data-acquisition times (134–136); the EECs obtained earlier were recently found to be significantly different from the those obtained by truly time-resolved 2-FTEIS methods (43, 48). EIS measurements have also played an important roles in photoelectrochemistry; recent reports in this area address the modeling of EECs for dye-sensitized solar cells (139–142), characterization of electron-transport properties (142, 143), properties of semiconductor–conducting polymer interfaces (144), and correlations between solar cell performances and EIS results (145). Finally, we give a few examples of the numerous EIS studies conducted on batteries and fuel cells. These EIS studies have provided solutions to difficult problems such as (*a*) the intercalation of Li^+ into anode (146) and cathode (147) materials of rechargeable lithium batteries and (*b*) the charge-transfer and mass-transport behaviors of solid oxide (148) and polymer electrolyte membrane (149, 150) fuel cells.

5. CONCLUSIONS

In this review we have described recent progress in EIS measurement techniques, the science related to the electrified interfaces according to results obtained with new techniques, and novel interpretations and approaches to solving various electrochemical problems. The FTEIS techniques, particularly 2-FTEIS, provide rich information about electrochemical systems at electrified interfaces, allowing their complete descriptions to be made. The short measurement time for the FTEIS method permits impedance measurements to be made in real time for many electrochemical systems, which has allowed many complex electrochemical reactions and interfacial phenomena to be solved. Also, the high data-acquisition rate for EIS spectra should lead to the effective impedance mapping of electrically heterogeneous surfaces in the not-too-distant future.

Particularly important is the conclusion, obtained from the current expression derived from the EEC, that the EEC represents a true model for an electrochemical interface and the reaction taking place thereat. Further, new results on time constants for electrochemical systems, in which polarization resistances take part in determining them (particularly at high overpotentials), are significant.

Another important recent development in EIS is its use as a label-free detection tool for many biosensors. Appropriate surface modification allows the electrode to selectively interact with target

analytes or to form host-guest complexes; these analytes include large biological compounds such as proteins, DNA, cells, and trace amounts of heavy metal ions, as well as biological cells and bacteria. EIS sensitively analyzes the interactions of modified electrodes with analytes, producing measurable electric signals. The fact that EIS is capable of more sensitive detection than either voltammetric or amperometric methods is very significant (61, 62). Also, the measurement rate of 2-FTEIS should enable use of this technique as a detection tool for an array of hundreds of electrodes on, for example, DNA or other biochips in a short time as long as a reasonably reversible redox probe is employed.

The new FTEIS techniques are expected to elucidate various unsolved problems in electrochemistry. Novel experiments that were thought to be difficult, if not impossible, to perform without the new FTEIS techniques should be explored in order to solve complex problems encountered during the studies on electrochemical energy conversion, biosensors, and other materials-related areas.

DISCLOSURE STATEMENT

The authors are not aware of any affiliations, memberships, funding, or financial holdings that might be perceived as affecting the objectivity of this review.

ACKNOWLEDGMENTS

Our work was supported by the World Class University program funded by the Korea Research Foundation to the Ulsan National Institute of Science and Technology.

LITERATURE CITED

1. Macdonald DD. 2006. Reflections on the history of electrochemical impedance spectroscopy. *Electrochim. Acta* 51:1376–88
2. Randles JEB. 1947. Kinetics of rapid electrode reactions. *Discuss. Faraday Soc.* 1:11–19
3. Bard AJ, Faulkner LR. 2001. Polarography and pulse voltammetry. In *Electrochemical Methods: Fundamentals and Applications*, pp. 261–304. New York: Wiley
4. Park SM, Yoo JS. 2003. Electrochemical impedance spectroscopy for better electrochemical measurements. *Anal. Chem.* 75:A455–81
5. Orazem ME, Tribollet B. 2008. *Electrochemical Impedance Spectroscopy*. Hoboken, NJ: Wiley
6. Panke O, Balkenhohl T, Kafka J, Schafer D, Lisdat F. 2008. Impedance spectroscopy and biosensing. *Adv. Biochem. Eng. Biotechnol.* 109:195–237
7. Bao N, Wang J, Lu C. 2008. Recent advances in electric analysis of cells in microfluidic systems. *Anal. Bioanal. Chem.* 391:933–42
8. Lisdat F, Schafer D. 2008. The use of electrochemical impedance spectroscopy for biosensing. *Anal. Bioanal. Chem.* 391:1555–67
9. Lieberzeit PA, Dickert FL. 2008. Rapid bioanalysis with chemical sensors: novel strategies for devices and artificial recognition membranes. *Anal. Bioanal. Chem.* 391:1629–39
10. Qavi AJ, Washburn AL, Byeon JY, Bailey RC. 2009. Label-free technologies for quantitative multiparameter biological analysis. *Anal. Bioanal. Chem.* 394:121–35
11. Bogomolova A, Komarova E, Reber K, Gerasimov T, Yavuz O, et al. 2009. Challenges of electrochemical impedance spectroscopy in protein biosensing. *Anal. Chem.* 81:3944–49
12. Daniels JS, Pourmand N. 2007. Label-free impedance biosensors: opportunities and challenges. *Electroanalysis* 19:1239–57
13. Pejcic B, De Marco R. 2006. Impedance spectroscopy: over 35 years of electrochemical sensor optimization. *Electrochim. Acta* 51:6217–29

14. Huang QA, Hui R, Wang BW, Zhang HJ. 2007. A review of ac impedance modeling and validation in SOFC diagnosis. *Electrochim. Acta* 52:8144–64
15. Sluyters-Rehbach M, Sluyters JH. 1979. On the meaning of the impedance concept in the case of an object that varies with time and in the case of a swept frequency. *J. Electroanal. Chem.* 102:415–19
16. Popkirov GS, Schneider RN. 1993. Validation of experimental data in electrochemical impedance spectroscopy. *Electrochim. Acta* 38:861–67
17. Stoynov ZB, Savova-Stoynov BS. 1985. Impedance study of nonstationary systems: four-dimensional analysis. *J. Electroanal. Chem.* 183:133–44
18. Savova-Stoynov BS, Stoynov ZB. 1992. Four-dimensional estimation of the instantaneous impedance. *Electrochim. Acta* 37:2353–55
19. Stoynov Z. 1992. Rotating Fourier transform—new mathematical basis for nonstationary impedance analysis. *Electrochim. Acta* 37:2357–59
20. Stoynov Z. 1993. Nonstationary impedance spectroscopy. *Electrochim. Acta* 38:1919–22
21. Smith DE. 1976. The acquisition of electrochemical response spectra by on-line fast Fourier transform. Data processing in electrochemistry. *Anal. Chem.* 48:A221–40
22. Jeno H, Elton DM, Czerwinski WA, Schiewe JG, Vicente-Beckett VA, Bond AM. 1997. Microcomputer-based instrumentation for multi-frequency Fourier transform alternating current (admittance and impedance) voltammetry. *J. Electroanal. Chem.* 437:1–15
23. Ühlken J, Waser R, Wiese H. 1988. Fourier transform impedance spectrometer using logarithmically spaced time samples. *Ber. Bunsenges. Phys. Chem.* 92:730–35
24. Házì J, Elton DM, Czerwinski WA, Schiewe J, Beckett VA, Bond AM. 1997. Microcomputer-based instrumentation for multi-frequency Fourier transform alternating current (admittance and impedance) voltammetry. *J. Electroanal. Chem.* 437:1–15
25. Popkirov GS, Schindler RN. 1992. A new impedance spectrometer for the investigation of electrochemical systems. *Rev. Sci. Instrum.* 63:5366–72
26. Baranski AS, Krogulec T, Nelson LJ, Norouzi P. 1998. High-frequency impedance spectroscopy of platinum ultramicroelectrodes in flowing solutions. *Anal. Chem.* 70:2895–901
27. Rosvall M, Sharp M. 2000. A complete system for electrochemical impedance spectroscopy which combines FFT methods and staircase voltammetry. *Electrochem. Comm.* 2:338–43
28. Darowicki K, Orlikowski J, Lentka G. 2000. Instantaneous impedance spectra of a nonstationary model electrical system. *J. Electroanal. Chem.* 486:106–10
29. Darowicki K, Slepski P. 2002. Influence of the analyzing window on electrode impedance measurement by the continuous frequency scanning method. *J. Electroanal. Chem.* 533:25–31
30. Darowicki K, Slepski P. 2003. Dynamic electrochemical impedance spectroscopy of the first order electrode reaction. *J. Electroanal. Chem.* 547:1–8
31. Darowicki K, Orlikowski J, Arutunow A, Jurczak W. 2007. Comparative electrochemical analysis of the passive layer cracking process on aluminum alloys performed by means of dc and ac techniques. *J. Electrochem. Soc.* 154:C74–80
32. Arutunow A, Darowicki K. 2008. DEIS assessment of AISI 304 stainless steel dissolution process in conditions of intergranular corrosion. *Electrochim. Acta* 53:4387–95
33. Arutunow A, Darowicki K. 2009. DEIS evaluation of the relative effective surface area of AISI 304 stainless steel dissolution process in conditions of intergranular corrosion. *Electrochim. Acta* 54:1034–41
34. Darowicki K, Andrearczyk K. 2009. Determination of occurrence of anodic excursion peaks by dynamic electrochemical impedance spectroscopy, atomic force microscopy and cyclic voltammetry. *J. Power Sources* 189:988–93
35. Darowicki K, Szocinski M. 2007. Local impedance spectroscopy of membranes. *J. Membr. Sci.* 303:1–5
36. Garland JE, Assiongbon KA, Pettit CM, Emery SB, Roy D. 2002. Kinetic analysis of electrosorption using fast Fourier transform electrochemical impedance spectroscopy: underpotential deposition of Bi^{3+} in the presence of coadsorbing $ClO4^{-}$ on gold. *Electrochim. Acta* 47:4113–24
37. Garland JE, Pettit CM, Roy D. 2004. Analysis of experimental constraints and variables for time resolved detection of Fourier transform electrochemical impedance spectra. *Electrochim. Acta* 49:2623–35

38. Pettit CM, Goonetilleke PC, Sulyma CM, Roy D. 2006. Combining impedance spectroscopy with cyclic voltammetry: measurement and analysis of kinetic parameters for faradaic and nonfaradaic reactions on thin-film gold. *Anal. Chem.* 78:3723–29
39. Ragoisha GA, Bondarenko AS. 2005. Potentiodynamic electrochemical impedance spectroscopy. *Electrochim. Acta* 50:1553–63
40. Bondarenko A, Ragoisha G. 2005. Variable Mott-Schottky plots acquisition by potentiodynamic electrochemical impedance spectroscopy. *J. Solid State Electrochem.* 9:845–49
41. Bondarenko AS, Ragoisha GA, Osipovich NP, Streltsov EA. 2005. Potentiodynamic electrochemical impedance spectroscopy of lead UPD on polycrystalline gold and on selenium atomic underlayer. *Electrochem. Comm.* 7:631–36
42. Yoo JS, Park SM. 2000. An electrochemical impedance measurement technique employing Fourier transform. *Anal. Chem.* 72:2035–41
43. Yoo JS, Song I, Lee JH, Park SM. 2003. Real-time impedance measurements during electrochemical experiments and their application to aniline oxidation. *Anal. Chem.* 75:3294–300
44. Park SM, Yoo JS, Chang BY, Ahn ES. 2006. Novel instrumentation in electrochemical impedance spectroscopy and a full description of an electrochemical system. *Pure Appl. Chem.* 78:1069–80
45. Chang BY, Park SM. 2006. Integrated description of electrode/electrolyte interfaces based on equivalent circuits and its verification using impedance measurements. *Anal. Chem.* 78:1052–60
46. Chang BY, Hong SY, Yoo JS, Park SM. 2006. Determination of electron transfer kinetic parameters by Fourier transform electrochemical impedance spectroscopic analysis. *J. Phys. Chem. B* 110:19386–92
47. Chang BY, Park SM. 2007. Fourier transform analysis of chronoamperometric currents obtained during staircase voltammetric experiments. *Anal. Chem.* 79:4892–99
48. Hong SY, Park SM. 2007. Electrochemistry of conductive polymers. 40. Earlier phases of aniline polymerization studied by Fourier transform electrochemical impedance spectroscopy. *J. Phys. Chem. B* 111:9779–86
49. Park JB, Chang BY, Yoo JS, Hong SY, Park SM. 2007. Resolution of a multi-step electron transfer reaction by time resolved impedance measurements: sulfur reduction in nonaqueous media. *Bull. Korean Chem. Soc.* 28:1523–30
50. Chang BY, Ahn E, Park SM. 2008. Real-time staircase cyclic voltammetry Fourier transform electrochemical impedance spectroscopic studies on underpotential deposition of lead on gold. *J. Phys. Chem. C* 112:16902–9
51. Mozaffari SA, Chang T, Park SM. 2009. Diffusional electrochemistry of cytochrome *c* on mixed captopril/3-mercapto-1-propanol self-assembled monolayer modified gold electrode. *J. Phys. Chem. C* 113:12434–42
52. Juraczakowski R, Lasia A. 2004. Limitations of the potential step technique to impedance measurements using discrete time Fourier transform. *Anal. Chem.* 76:5033–38
53. Urquidi-Macdonald M, Real S, Macdonald DD. 1990. Applications of Kramers-Krönig transforms in the analysis of electrochemical impedance data. III. Stability and linearity. *Electrochim. Acta* 35:1559–66
54. Osteryoung J. 1993. Voltammetry for the future. *Acc. Chem. Res.* 26:77–83
55. Delahay P. 1953. Unified theory of polarographic waves. *J. Am. Chem. Soc.* 75:1430–35
56. Pilla A. 1970. A transient impedance technique for the study of electrode kinetics. *J. Electrochem. Soc.* 117:467–77
57. Smyrl W. 1985. Digital impedance for faradaic analysis. *J. Electrochem. Soc.* 132:1551–55
58. Takano K, Nozaki K, Saito Y, Kato K, Negishi A. 2000. Impedance spectroscopy by voltage-step chronoamperometry using the Laplace transform method in a lithium-ion battery. *J. Electrochem. Soc.* 147:922–29
59. Barsoukov E, Ryu SH, Lee H. 2002. A novel impedance spectrometer based on carrier function Laplace-transform of the response to arbitrary excitation. *J. Electroanal. Chem.* 536:109–22
60. Onda K, Nakayama M, Fukuda K, Wakahara K, Arakai T. 2006. Cell impedance measurement by Laplace transformation of charge or discharge current-voltage. *J. Electrochem. Soc.* 153:A1012–18
61. Park JY, Lee YS, Chang BY, Karthikeyan S, Kim KS, et al. 2009. (*R*)-lipo-diaza-18-crown-6 self-assembled monolayer as a selective serotonin receptor. *Anal. Chem.* 81:3843–50

62. Park JY, Chang BY, Nam H, Park SM. 2008. Selective electrochemical sensing of glycated hemoglobin (HbA_{1c}) on thiophene-3–boronic acid self-assembled monolayer covered gold electrodes. *Anal. Chem.* 80:8035–44
63. Horvat-Radosevic V, Kvastek K, Kraljic-Rokovic M. 2006. Impedance spectroscopy of oxidized polyaniline and poly(o-ethoxyaniline) thin film modified Pt electrodes. *Electrochim. Acta* 51:3417–28
64. Ragoisha GA, Bondarenko AS, Osipovich NP, Rabchynski SM, Streltsov EA. 2008. Multiparametric characterization of metal-chalcogen atomic multilayer assembly by potentiodynamic electrochemical impedance spectroscopy. *Electrochim. Acta* 53:3879–88
65. Ragoisha GA, Bondarenko AS, Osipovich NP, Streltsov EA. 2004. Potentiodynamic electrochemical impedance spectroscopy: lead underpotential deposition on tellurium. *J. Electroanal. Chem.* 565:227–34
66. Blajiev OL, Breugelmans T, Pintelon R, Terryn H, Hubin A. 2008. Potentiodynamic EIS investigation of the 2-methyl-5-mercapto-1,3,4-thiadiazole adsorption on copper. *Electrochim. Acta* 53:7451–59
67. Hong Y, Patri UB, Ramakrishnan S, Roy D, Babu SV. 2005. Utility of dodecyl sulfate surfactants as dissolution inhibitors in chemical mechanical planarization of copper. *J. Mater. Res.* 20:3413–24
68. Pettit CM, Goonetilleke PC, Roy D. 2006. Measurement of differential capacitance for faradaic systems under potentiodynamic conditions: considerations of Fourier transform and phase-selective techniques. *J. Electroanal. Chem.* 589:219–31
69. Nagarajan S, Karthega M, Rajendran N. 2007. Pitting corrosion studies of super austenitic stainless steels in natural sea water using dynamic electrochemical impedance spectroscopy. *J. Appl. Electrochem.* 37:195–201
70. Ciubotariu A-C, Benea L, Lakatos-Varsanyi M, Dragan V. 2008. Electrochemical impedance spectroscopy and corrosion behavior of Al_2O_3-Ni nano composite coatings. *Electrochim. Acta* 53:4557–63
71. Nagarajan S, Rajendran N. 2009. Crevice corrosion behavior of superaustenitic stainless steels: dynamic electrochemical impedance spectroscopy and atomic force microscopy studies. *Corros. Sci.* 51:217–24
72. Zheng JP, Klug BK, Roy D. 2008. Electrochemical investigation of surface reactions for chemical mechanical planarization of tantalum in oxalic acid solutions. *J. Electrochem. Soc.* 155:H341–50
73. Leisner M, Carstensen J, Foll H. 2008. FFT impedance spectroscopy analysis of the growth of anodic oxides on (100) p-Si for various solvents. *J. Electroanal. Chem.* 615:124–34
74. Carstensen J, Foca E, Keipert S, Foell H, Leisner M, Cojocaru A. 2008. New modes of FFT impedance spectroscopy applied to semiconductor pore etching and materials characterization. *Phys. Status Solidi A* 205:2485–503
75. Foca E, Carstensen J, Popkirov G, Foll H. 2007. Pores growth control by in-situ FFT impedance spectroscopy. *Phys. Status Solidi A* 204:1378–82
76. Lillard RS, Moran PJ, Isaacs HS. 1992. A novel method for generating quantitative local electrochemical impedance spectroscopy. *J. Electrochem. Soc.* 139:1007–12
77. Zou F, Thierry D, Isaacs HS. 1997. A high-resolution probe for localized electrochemical impedance spectroscopy measurements. *J. Electrochem. Soc.* 144:1957–65
78. Annergren I, Zou F, Thierry D. 1999. Application of localised electrochemical techniques to study kinetics of initiation and propagation during pit growth. *Electrochim. Acta* 44:4383–93
79. Jorcin JB, Aragon E, Merlatti C, Pebere N. 2006. Delaminated areas beneath organic coating: a local electrochemical impedance approach. *Corros. Sci.* 48:1779–90
80. Frateur I, Huang VM, Orazem ME, Tribollet B, Vivier V. 2007. Experimental issues associated with measurement of local electrochemical impedance. *J. Electrochem. Soc.* 154:C719–27
81. Ervin EN, White HS, Baker LA. 2005. Alternating current impedance imaging of membrane pores using scanning electrochemical microscopy. *Anal. Chem.* 77:5564–69
82. Ervin EN, White HS, Baker LA, Martin CR. 2006. Alternating current impedance imaging of high-resistance membrane pores using a scanning electrochemical microscope. Application of membrane electrical shunts to increase measurement sensitivity and image contrast. *Anal. Chem.* 78:6535–41
83. Diakowski PM, Baranski AS. 2006. Positive and negative ac impedance feedback observed above conductive substrates under SECM conditions. *Electrochim. Acta* 52:854–62
84. Eckhard K, Kranz C, Shin H, Mizaikoff B, Schuhmann W. 2007. Frequency dependence of the electrochemical activity contrast in ac-scanning electrochemical microscopy and atomic force microscopy-ac-scanning electrochemical microscopy imaging. *Anal. Chem.* 79:5435–38

85. Eckhard K, Schuhmann W. 2008. Alternating current techniques in scanning electrochemical microscopy (AC-SECM). *Analyst* 133:1486–97
86. Eckhard K, Erichsen T, Stratmann M, Schuhmann W. 2008. Frequency-dependent alternating-current scanning electrochemical microscopy (4D AC-SECM) for local visualisation of corrosion sites. *Chem. Eur. J.* 14:3968–76
87. Layson A, Gadad S, Teeters D. 2003. Resistance measurements at the nanoscale: scanning probe ac impedance spectroscopy. *Electrochim. Acta* 48:2207–13
88. O'Hayre R, Lee M, Prinz FB. 2004. Ionic and electronic impedance imaging using atomic force microscopy. *J. Appl. Phys.* 95:8382–92
89. Darowicki K, Zielinski A, Kurzydlowski KJ. 2008. Application of dynamic impedance spectroscopy to atomic force microscopy. *Sci. Technol. Adv. Mater.* 9:1–5
90. Schiller CA, Richter F, Gulzow E, Wagner N. 2001. Validation and evaluation of electrochemical impedance spectra of systems with states that change with time. *Phys. Chem. Chem. Phys.* 3:374–78
91. Ganesh V, Pandey RR, Malhotra BD, Lakshminarayanan V. 2008. Electrochemical characterization of self-assembled monolayers (SAMs) of thiophenol and aminothiophenols on polycrystalline Au: effects of potential cycling and mixed SAM formation. *J. Electroanal. Chem.* 619:87–97
92. Cho SH, Kim D, Park SM. 2008. Electrochemistry of conductive polymers. 41. Effects of self-assembled monolayers of aminophenols on polyaniline films. *Electrochim. Acta* 53:3820–27
93. Berggren C, Bjarnason B, Johansson G. 2001. Capacitive biosensors. *Electroanalysis* 13:173–80
94. Laczka O, Baldrich E, Munoz FX, del Campo FJ. 2008. Detection of *Escherichia coli* and *Salmonella typhimurium* using interdigitated microelectrode capacitive immunosensors: the importance of transducer geometry. *Anal. Chem.* 80:7239–47
95. Wang JB, Profitt JA, Pugia MJ, Suni II. 2006. Au nanoparticle conjugation for impedance and capacitance signal amplification in biosensors. *Anal. Chem.* 78:1769–73
96. Delaney TL, Zimin D, Rahm M, Weiss D, Wolfbeis OS, Mirsky VM. 2007. Capacitive detection in ultrathin chemosensors prepared by molecularly imprinted grafting photopolymerization. *Anal. Chem.* 79:3220–25
97. Huang Y, Bell MC, Suni II. 2008. Impedance biosensor for peanut protein Ara h 1. *Anal. Chem.* 80:9157–61
98. Park JY, Lee YS, Kim BH, Park SM. 2008. Label-free detection of antibody-antigen interactions on (*R*)-lipo-diaza-18-crown-6 self-assembled monolayer modified gold electrodes. *Anal. Chem.* 80:4986–93
99. Chen XJ, Wang YY, Zhou JJ, Yan W, Li XH, Zhu JJ. 2008. Electrochemical impedance immunosensor based on three-dimensionally ordered macroporous gold film. *Anal. Chem.* 80:2133–40
100. Yeo J, Park JY, Bae WJ, Lee YS, Kim BH, et al. 2009. Label-free electrochemical detection of the p53 core domain protein on its antibody immobilized electrode. *Anal. Chem.* 81:4770–77
101. Tsekenis G, Garifallou GZ, Davis F, Millner PA, Gibson TD, Higson SPJ. 2008. Label-less immunosensor assay for myelin basic protein based upon an ac impedance protocol. *Anal. Chem.* 80:2058–62
102. Barton AC, Davis F, Higson SPJ. 2008. Labeless immunosensor assay for prostate specific antigen with picogram per milliliter limits of detection based upon an ac impedance protocol. *Anal. Chem.* 80:6198–205
103. Yang LMC, Diaz JE, McIntire TM, Weiss GA, Penner RM. 2008. Direct electrical transduction of antibody binding to a covalent virus layer using electrochemical impedance. *Anal. Chem.* 80:5695–705
104. O'Grady ML, Parker KK. 2008. Dynamic control of protein-protein interactions. *Langmuir* 24:316–22
105. Maalouf R, Fournier-Wirth C, Coste J, Chebib H, Saikali Y, et al. 2007. Label-free detection of bacteria by electrochemical impedance spectroscopy: comparison to surface plasmon resonance. *Anal. Chem.* 79:4879–86
106. Mantzila AG, Maipa V, Prodromidis MI. 2008. Development of a faradic impedimetric immunosensor for the detection of *Salmonella typhimurium* in milk. *Anal. Chem.* 80:1169–75
107. Qiu Y, Liao R, Zhang X. 2009. Impedance-based monitoring of ongoing cardiomyocyte death induced by tumor necrosis factor–α. *Biophys. J.* 96:1985–91
108. Tsekenis G, Garifallou GZ, Davis F, Millner PA, Pinacho DG, et al. 2008. Detection of fluoroquinolone antibiotics in milk via a labelless immunoassay based upon an alternating current impedance protocol. *Anal. Chem.* 80:9233–39

109. Barton AC, Collyer SD, Davis F, Garifallou GZ, Tsekenis G, et al. 2009. Labeless ac impedimetric antibody-based sensors with pg ml^{-1} sensitivities for point-of-care biomedical applications. *Biosens. Bioelectron.* 24:1090–95
110. Park JY, Kim BC, Park SM. 2007. Molecular recognition of protonated polyamines at calix[4]crown-5 self-assembled monolayer modified electrodes by impedance measurements. *Anal. Chem.* 79:1890–96
111. Mahmoud KA, Luong JHT. 2008. Impedance method for detecting HIV-1 protease and screening for its inhibitors using ferrocene-peptide conjugate/Au nanoparticle/single-walled carbon nanotube modified electrode. *Anal. Chem.* 80:7056–62
112. Drummond TG, Hill MG, Barton JK. 2003. Electrochemical DNA sensors. *Nat. Biotechnol.* 21:1192–99
113. Vagin MY, Trashin SA, Karyakin AA, Mascini M. 2008. Label-free detection of DNA hybridization at a liquid-liquid interface. *Anal. Chem.* 80:1336–40
114. Manesse M, Stambouli V, Boukherroub R, Szunerits S. 2008. Electrochemical impedance spectroscopy and surface plasmon resonance studies of DNA hybridization on gold/SiO_x interfaces. *Analyst* 133:1097–103
115. Li XH, Lee JS, Kraatz HB. 2006. Electrochemical detection of single-nucleotide mismatches using an electrode microarray. *Anal. Chem.* 78:6096–101
116. Wang Y, Li CJ, Li XH, Li YF, Kraatz HB. 2008. Unlabeled hairpin-DNA probe for the detection of single-nucleotide mismatches by electrochemical impedance spectroscopy. *Anal. Chem.* 80:2255–60
117. Li XH, Song HF, Nakatani K, Kraatz HB. 2007. Exploiting small molecule binding to DNA for the detection of single-nucleotide mismatches and their base environment. *Anal. Chem.* 79:2552–55
118. Park JY, Kwon SH, Park JW, Park SM. 2008. Label-free detection of DNA molecules on the dendron based self-assembled monolayer by electrochemical impedance spectroscopy. *Anal. Chim. Acta* 619:37–42
119. Li C-Z, Liu Y, Luong JHT. 2005. Impedance sensing of DNA binding drugs using gold substrates modified with gold nanoparticles. *Anal. Chem.* 77:478–85
120. Ghanbari K, Bathaie SZ, Mousavi MF. 2008. Electrochemically fabricated polypyrrole nanofiber–modified electrode as a new electrochemical DNA biosensor. *Biosens. Bioelectron.* 23:1825–31
121. Radi A-E, Acero Sanchez JL, Baldrich E, O'Sullivan CK. 2005. Reusable impedimetric aptasensor. *Anal. Chem.* 77:6320–23
122. Li XX, Shen LH, Zhang DD, Qi HL, Gao Q, et al. 2008. Electrochemical impedance spectroscopy for study of aptamer-thrombin interfacial interactions. *Biosens. Bioelectron.* 23:1624–30
123. Xu Y, Yang L, Ye XY, He PA, Fang YZ. 2006. An aptamer-based protein biosensor by detecting the amplified impedance signal. *Electroanalysis* 18:1449–56
124. Lee JA, Hwang S, Kwak J, Park SI, Lee SS, Lee K-C. 2008. An electrochemical impedance biosensor with aptamer-modified pyrolyzed carbon electrode for label-free protein detection. *Sens. Actuators B* 129:372–79
125. Willner I, Zayats M. 2007. Electronic aptamer-based sensors. *Angew. Chem. Int. Ed.* 46:6408–18
126. de-los-Santos-Álvareza N, Lobo-Castañóna MaJ, Miranda-Ordieresa AJ, Tuñón-Blanco P. 2008. Aptamers as recognition elements for label-free analytical devices. *Trends Anal. Chem.* 27:437–46
127. Cai M, Park SM. 1996. Oxidation of zinc in alkaline solutions studied by electrochemical impedance spectroscopy. *J. Electrochem. Soc.* 143:3895–902
128. Sherif EM, Park SM. 2006. Effects of 1,4-naphthoquinone on aluminum corrosion in 0.50 M sodium chloride solutions. *Electrochim. Acta* 51:1313–21
129. Sherif EM, Park SM. 2006. Inhibition of copper corrosion in acidic pickling solutions by N-phenyl-1,4-phenylenediamine. *Electrochim. Acta* 51:4665–73
130. Sherif EM, Park SM. 2006. Effects of 2-amino-5-ethylthio-1,3,4-thiadiazole on copper corrosion as a corrosion inhibitor in aerated acidic pickling solutions. *Electrochim. Acta* 51:6556–62
131. Sherif EM, Park SM. 2006. 2-Amino-5-ethyl-1,3,4-thiadiazole as a corrosion inhibitor for copper in 3.0% NaCl solutions. *Corros. Sci.* 51:4665–73
132. Scully JR. 2000. Polarization resistance method for determination of instantaneous corrosion rates. *Corrosion* 56:199–218
133. Mansfeld F. 1995. Use of electrochemical impedance spectroscopy for the study of corrosion protection by polymer coatings. *J. Appl. Electrochem.* 25:187–202

134. Johnson BJ, Park SM. 1996. Electrochemistry of conductive polymers. XIX. Oxidation of aniline at bare and polyaniline-modified electrodes studied by electrochemical impedance spectroscopy. *J. Electrochem. Soc.* 143:1269–76
135. Sarac AS, Ates M, Kilic B. 2008. Electrochemical impedance spectroscopic study of polyaniline on platinum, glassy carbon and carbon fiber microelectrodes. *Int. J. Electrochem. Sci.* 3:777–86
136. Bardavid Y, Ghabboun J, Porath D, Kotylar AB, Yitzchaik S. 2008. Formation of polyaniline layer on DNA by electrochemical polymerization. *Polymer* 49:2217–22
137. Horvat-Radosevic V, Kvastek K. 2009. Three-electrode cell set-up electrical equivalent circuit applied to impedance analysis of thin polyaniline film modified electrodes. *J. Electroanal. Chem.* 631:10–21
138. Fernandez-Sanchez C, McNeil CJ, Rawson K. 2005. Electrochemical impedance spectroscopy studies of polymer degradation: application to biosensor development. *Trends Anal. Chem.* 24:37–48
139. Han LY, Koide N, Chiba Y, Mitate T. 2004. Modeling of an equivalent circuit for dye-sensitized solar cells. *Appl. Phys. Lett.* 84:2433–35
140. Wang Q, Moser JE, Gratzel M. 2005. Electrochemical impedance spectroscopic analysis of dye-sensitized solar cells. *J. Phys. Chem. B* 109:14945–53
141. Fabregat-Santiago F, Bisquert J, Garcia-Belmonte G, Boschloo G, Hagfeldt A. 2005. Influence of electrolyte in transport and recombination in dye-sensitized solar cells studied by impedance spectroscopy. *Solar Energy Mater. Solar Cells* 87:117–31
142. Ku CH, Wu JJ. 2007. Electron transport properties in ZnO nanowire array/nanoparticle composite dye-sensitized solar cells. *Appl. Phys. Lett.* 91:093117
143. He C, Zheng Z, Tang HL, Zhao LN, Lu F. 2009. Electrochemical impedance spectroscopy characterization of electron transport and recombination in ZnO nanorod dye-sensitized solar cells. *J. Phys. Chem. C* 113:10322–25
144. Mani A, Huisman C, Goossens A, Schoonman J. 2008. Mott-Schottky analysis and impedance spectroscopy of TiO_2/6T and ZnO/6T devices. *J. Phys. Chem. B* 112:10086–91
145. Fabregat-Santiago F, Bisquert J, Palomares E, Otero L, Kuang DB, et al. 2007. Correlation between photovoltaic performance and impedance spectroscopy of dye-sensitized solar cells based on ionic liquids. *J. Phys. Chem. C* 111:6550–60
146. Paio T, Park SM, Doh CH, Moon SI. 1999. Intercalation of lithium ions into graphite electrodes studied by ac impedance measurements. *J. Electrochem. Soc.* 146:2794–98
147. Lu DS, Li WS, Zuo XX, Yuan ZZ, Huang Q. 2007. Study on electrode kinetics of Li^+ insertion in $Li_xMn_2O_4$ ($0 \leq x \leq 1$) by electrochemical impedance spectroscopy. *J. Phys. Chem. C* 111:12067–74
148. Kato T, Nozaki K, Negishi A, Kato K, Monma A, et al. 2004. Impedance analysis of a disk-type SOFC using doped lanthanum gallate under power generation. *J. Power Sources* 133:169–74
149. Malevich D, Halliop E, Peppley BA, Pharoah JG, Karan K. 2009. Investigation of charge-transfer and mass-transport resistances in PEMFCs with microporous layer using electrochemical impedance spectroscopy. *J. Electrochem. Soc.* 156:B216–24
150. Danzer MA, Hofer EP. 2009. Analysis of the electrochemical behavior of polymer electrolyte fuel cells using simple impedance models. *J. Power Sources* 190:25–33

Annual Review of
Analytical Chemistry

Volume 3, 2010

Contents

Indexes

Errata

An online log of corrections to *Annual Review of Analytical Chemistry* articles may be found at http://arjournals.annualreviews.org/errata/anchem.